

Two statistical regimes in the transition to filamentation

Alexis Gomel,^{1,2} Geoffrey Gaulier,¹ Debbie Eeltink,^{1,2,3} Maura Brunetti,^{1,4} and Jérôme Kasparian ^{1,2,*}

¹*Group of Applied Physics, University of Geneva, 1205 Geneva, Switzerland*

²*Institute for Environmental Sciences, University of Geneva, 1205 Geneva, Switzerland*

³*Present address: Laboratory of Theoretical Physics of Nanosystems, EPFL, Ch-1015 Lausanne, 10 Switzerland*

⁴*Institute for Environmental Sciences, University of Geneva, 1205 Geneva, Switzerland*

Abstract

We experimentally investigate fluctuations in the spectrum of ultrashort laser pulses propagating in air, close to the critical power for filamentation. Increasing the laser peak power broadens the spectrum while the beam approaches the filamentation regime. We identify two regimes for this transition: In the center of the spectrum, the output spectral intensity increases continuously. In contrast, on the edges of the spectrum the transition implies a bimodal probability distribution function for intermediate incident pulse energies, where a high-intensity mode appears and grows at the expense of the original low-intensity mode. We argue that this dual behavior prevents the definition of a univoqual threshold for filamentation, shedding a new light on the long-standing lack of explicit definition of the boundary of the filamentation regime.

arXiv:2301.01971v1 [physics.optics] 5 Jan 2023

* jerome.kasparian@unige.ch

I. INTRODUCTION

Filamentation is a self-guided propagation regime typical of ultrashort, high-power laser pulses [1–4]. Beyond a critical power (3 GW in air), the Kerr effect balances diffraction. The beam then self-focuses until higher-order nonlinear defocusing effects like ionization or the saturation of the Kerr effect [5] come into play. The resulting dynamical balance gives rise to self-guided light structures known as filaments. Filaments can extend over atmospheric scale distances [6, 7], opening the way to various applications from remote sensing [8] to lightning control [9–14], THz generation [15–20], fog clearing [21, 22], or the triggering of condensation in sub-saturated atmospheres [8, 23, 24]. Filaments show very characteristic and even spectacular features, including long-distance propagation, bright light emission due to both plasma emission on the side and spectral broadening in the forward direction, and noise associated to the shockwave [25–27]. Together, these features give rise to the intuitive notion of a qualitatively distinct propagation regime. However, defining a clear threshold for the filamentation regime turns out to be difficult [28], especially in focused beams where linear propagation can be sufficient to reach the ionization threshold [29], and even produce a denser plasma than Kerr self-focusing does [30]. Similarly, along the propagation axis, defining the onset and end of filaments, and therefore their length, requires somewhat arbitrary choices.

Here, we statistically investigate the transition to filamentation. Shot-to-shot fluctuations of the spectral amplitudes of a high-power laser beam, whether filamenting or not, are known to display characteristic probability distribution functions (PDF): A regular probability distribution is observed in the center of the spectrum, while on its edge the distribution is long-tailed (optical rogue wave [31]) [32]. We extend this analysis to the sub-filamenting regime and to the transition to filamentation, in order to characterize how the statistics evolves when the incident power progressively reaches the critical power for filamentation. The evolution of spectral intensity PDFs turns out to display typical and contrasted signatures on the edges and in the center of the spectrum, respectively, suggesting that transition to filamentation cannot be characterized as a whole. By doing so, we suggest that the ambiguities in the definition of the limits of the filamentation regime are intrinsic to the physical process rather than instrumental or conceptual limitations, shedding a new light on the long-standing lack of explicit definition of the boundary of the filamentation regime.

II. EXPERIMENTAL SETUP

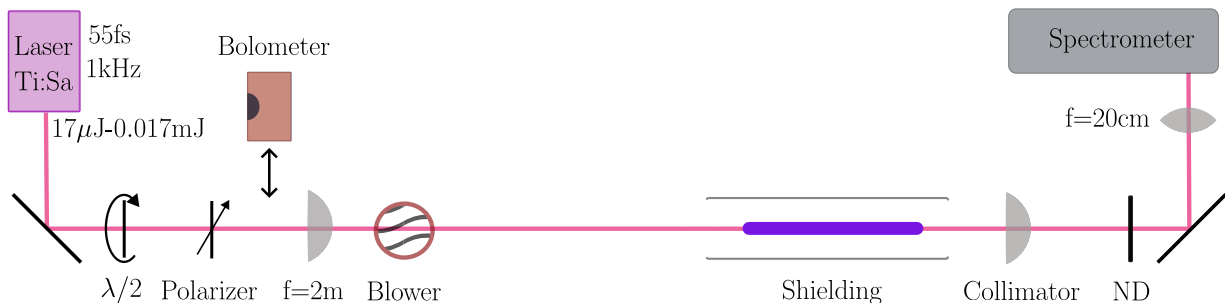


Figure 1. Experimental setup

The experimental setup (Figure 1) relied on a Coherent Astrella laser delivering ultrashort pulses at 1 kHz repetition rate. A half-wave plate installed in a motorized rotating stage ensuring $\pm 1^\circ$ precision, followed by a linear polarizer, allowed to adjust the pulse energy with an accuracy of $\sim 10 \mu\text{J}$. The angle-to-energy calibration was performed before each experimental run with a powermeter (Coherent PM10). The laser compressor was adjusted so as to slightly chirp the pulses to a duration of 55 fs (as measured with PulseCheck, APE Berlin), in order to reach the filamentation threshold in air within the tuning range of the energy. The beam was slightly focused from an initial diameter of 11 mm at $1/e^2$ by an $f = 2$ m BK7 plano-convex lens located approximately at 15 cm after the polarizer and subsequently through a 13.5 cm-long turbulent region generated by 48°C to 565°C hot air blown transversally by a hot air blower (Steinel HL1502 S). 15–27.5 cm downstream of the lens, the beam self-focused and filamentation started if the incident peak power was sufficient. The filamentation region was surrounded by a PVC tube of 18 cm diameter to shield the beam against air displacements in the room so as to improve its stability. After the end of filamentation region, the beam was imaged by a second BK7 lens ($f = 20$ cm) onto the entrance slit of an OceanOptics USB2000 spectrometer providing ~ 0.5 nm spectral resolution over the visible range. A neutral density filter prevented the spectrometer from saturating. The spectrum was measured and recorded independently for each laser shot. For each incident pulse

energy, 5000 individual spectra were recorded.

At each wavelength and incident energy, we characterized the shot to shot fluctuations by recording the PDF of the spectral intensity as a 100-bin histogram, using identical bins in all conditions to facilitate comparison. In the characterization of the PDF, we use among others Hogg's unbiased kurtosis estimator, defined as

$$Hg = \frac{U_{0.05} - L_{0.05}}{U_{0.5} - L_{0.5}} - 2.59 \quad (1)$$

where U_m and L_m refer to the mean of the upper and lower m quantiles, respectively. This means that $U_m = \frac{1}{m} \int_{1-m}^1 F^{-1}(y) dy$ and $L_m = \frac{1}{m} \int_0^m F^{-1}(y) dy$, where F is the cumulative distribution function. For a Gaussian PDF, the Hogg estimator is 0.

III. RESULTS AND DISCUSSION

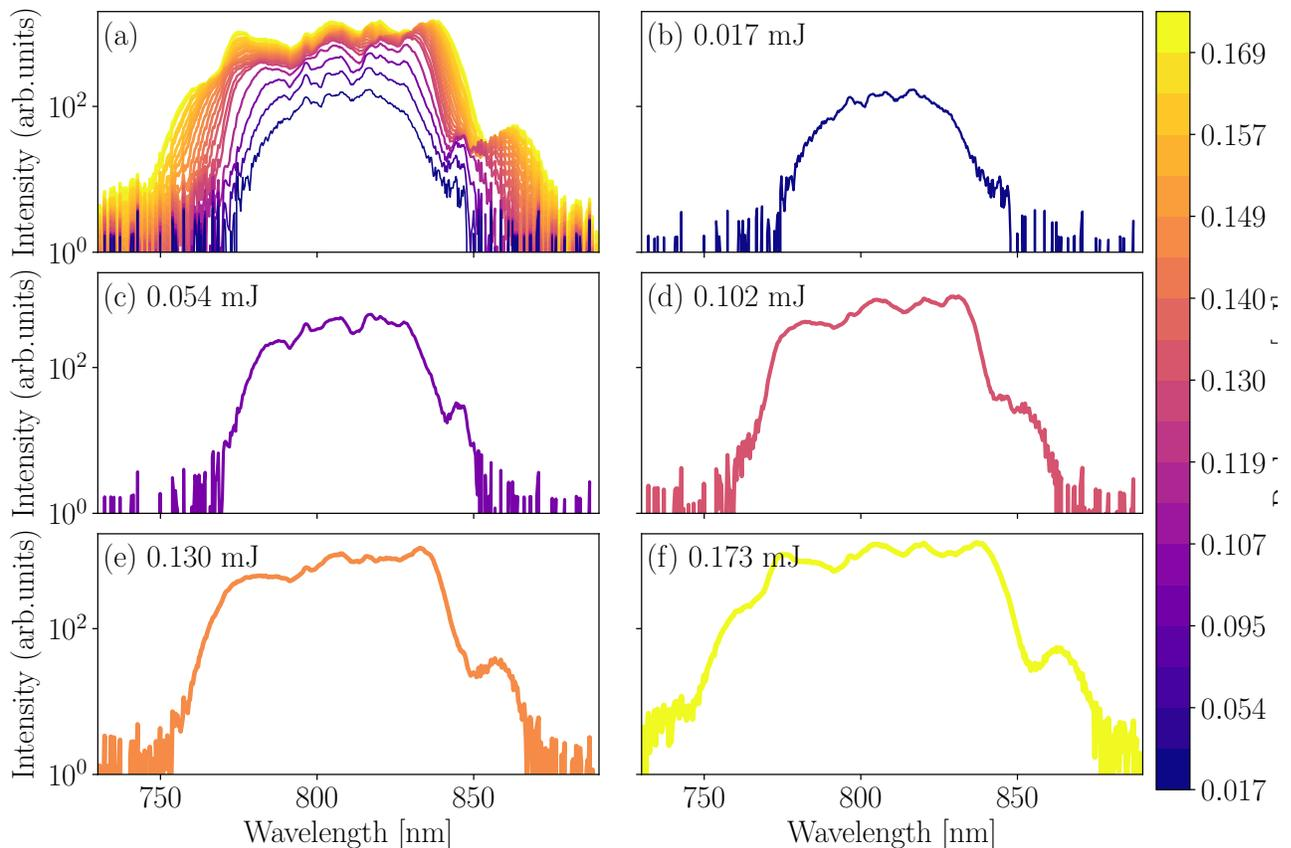


Figure 2. Evolution of the spectrum for increasing peak energy. (a) Average spectra; (b)-(f) Intensity fluctuations for incident pulse energies of 0.017, 0.054, 0.102, 0.130, and 0.173 mJ, respectively. In each panel, the solid thick line is the average intensity, the dark shaded area marks range between the 20th and the 80th percentiles and the light shaded area displays the range between the 5th and the 95th percentiles.

Figure 2a displays the evolution of the typical spectra recorded in the center of the beam after it starts diverging, for incident energies ranging from 0.017 to 0.173 mJ/pulse. The dark shaded area of Panels b-f encompasses the 20th to the 80th percentiles, while the light shadowed ranges from the 5th to the 95th ones, evidencing the typical range of the shot-to-shot fluctuations. As is typical for self-phase modulation (SPM) [32, 33], the spectral broadening

is characterized by the formation of an oscillatory plateau. For increasing incident powers, the plateau both rises in intensity and broadens by a progressive displacement of its edges away from the laser fundamental wavelength. Shot-to-shot fluctuations of the spectrum can therefore be characterized as essentially vertical (i.e., in intensity) in the central part of the spectrum, and essentially horizontal (i.e., in spectral range) on its edges.

As displayed in Figure 2b–f, the shot-to-shot fluctuations can have the same order of magnitude as the mean spectral intensity all over the spectrum. In particular, above the threshold for appreciable spectral broadening, fluctuations reach a factor of 4, ranging from the non-filamenting to the filamenting regimes even at average incident pulse energies up to the critical power (0.173 mJ, $P = 3.15 \text{ GW} \sim P_{\text{cr}}$) where the filamentation visually seems to be well established. Such behavior randomly alternating filamenting (spectrally broadened) and non-filamenting pulses is consistent with the previously observed effect of turbulence on filamentation [34–36]. These fluctuations stem from the pre-filamentation fluctuations of the incident laser itself and from the influence of the turbulence, as well as the nonlinear transformation of the spectrum performed by the spectral broadening in the high-intensity region of propagation.

The vertical and horizontal behaviors of the shot-to-shot fluctuations result in qualitatively different evolutions of the PDF as a function of incident energy (fig. 3). In the center of the spectrum (805 nm, panels g and h), increasing the incident pulse energy continuously shifts the peak of the PDF, from low to high spectral intensity. This shift becomes faster and faster when moving away from the center of the spectrum (See 785 nm, panels e and f). Reaching the spectrum edges, the behavior qualitatively changes, with the PDF becoming bimodal over the transition (773 nm, panels b,c, and 860 nm, panels i,j). Over the power range where the transition occurs, the low-intensity peak progressively vanishes, while the high-intensity peak emerges. This behavior develops over a spectral range of ~ 10 nm on each side of the spectrum. Even further on the edges (765 nm, panels a,b), the bimodal behavior disappears again. The PDF initially peaks close to zero intensity and rises when the broadening becomes sufficient.

Note that in spite of patterns visually similar to tipping points, these transitions cannot be described as such. Rather, each laser pulse is essentially an independent experiment, hitting a fresh parcel of air. This experiment therefore consists in a series of random probings of the system behavior, with random initial phase profiles. The qualitative behaviors associated to each incident pulse energy at each wavelength can be summarized in a “phase diagram” (fig. 4a). We identify the regions with negligible broadening, with fully deployed broadening, and two kinds of transition regions: either continuous or bimodal. Remarkably, the bimodal transition regions are characterized by a drop in both the skewness (fig. 4b) and Hogg’s unbiased kurtosis estimator H_g [37] (fig. 4c), while the continuous transitions are characterized by increasing skewness and H_g . This can be understood by considering the corresponding evolutions on fig. 3. In the central region of the spectrum, corresponding to continuous transitions, the PDF tail rises on the high-spectral intensity side, resulting in a heavier tail and growing asymmetry. In contrast, the appearance and growth of a secondary mode of the PDF tends to occur at the expense of the tails, and simultaneously results in a broadening of the central region of the PDF, which explains the smaller skewness and Hogg estimator. Further statistical moment like the kurtosis and coefficient of variation (i.e., the ratio between variance and mean) display qualitatively similar behaviors, as illustrated in fig. 5.

From a mechanistic point of view, the bimodal transition corresponds to the wavelength range where the evolution of the spectrum for increasing pulse energies mostly occurs as a horizontal fluctuation of the cliff delimiting the broadened spectrum, i.e., the creation of new frequencies that previously were virtually absent from the spectrum. At these wavelengths, the sharp rise of the spectrum (large $|\frac{dI}{dt}|$) followed by a relatively flat plateau of fluctuating width ensures the bimodal distribution, since the rising section of the spectrum has a negligible contribution to the PDF: The spectrum mainly features two ranges of attainable values, close to zero and on the plateau, respectively, while the intensity variations of the plateau itself is of second order. This interpretation also explains why the bimodal behavior is observed on a much narrower range of wavelengths around 850 nm (See fig. 4a), where the oscillation is sharper and the plateau is much less flat. In contrast, on the plateau, the fluctuations are mostly vertical. They consist in intensity fluctuations, i.e., an increased intensity of frequencies pre-existing in the incident pulse, so that the transition occurs continuously when the plateau progressively rises.

These two qualitatively different transition modes to a broadened pulse coexist in the evolution of the same spectrum, driven by the same self-phase modulation process, and only some nanometers apart. The discontinuous transition to filamentation on the edges of the spectrum where bimodal spectral intensity distributions are observed would point to a system where filamenting and non-filamenting regimes are qualitatively distinct, and co-exist over some range of input power. In contrast, the central part of the spectrum and its smooth, continuous transition would not allow to define a threshold for the filamenting regime. Note that this spectral range bears most of the pulse energy.

We argue that this dual behavior within the same spectrum during the transition to filamentation intrinsically prevents an unambiguous definition of the edges of a filamenting regime that would be qualitatively different from an essentially linear extended focus [29].

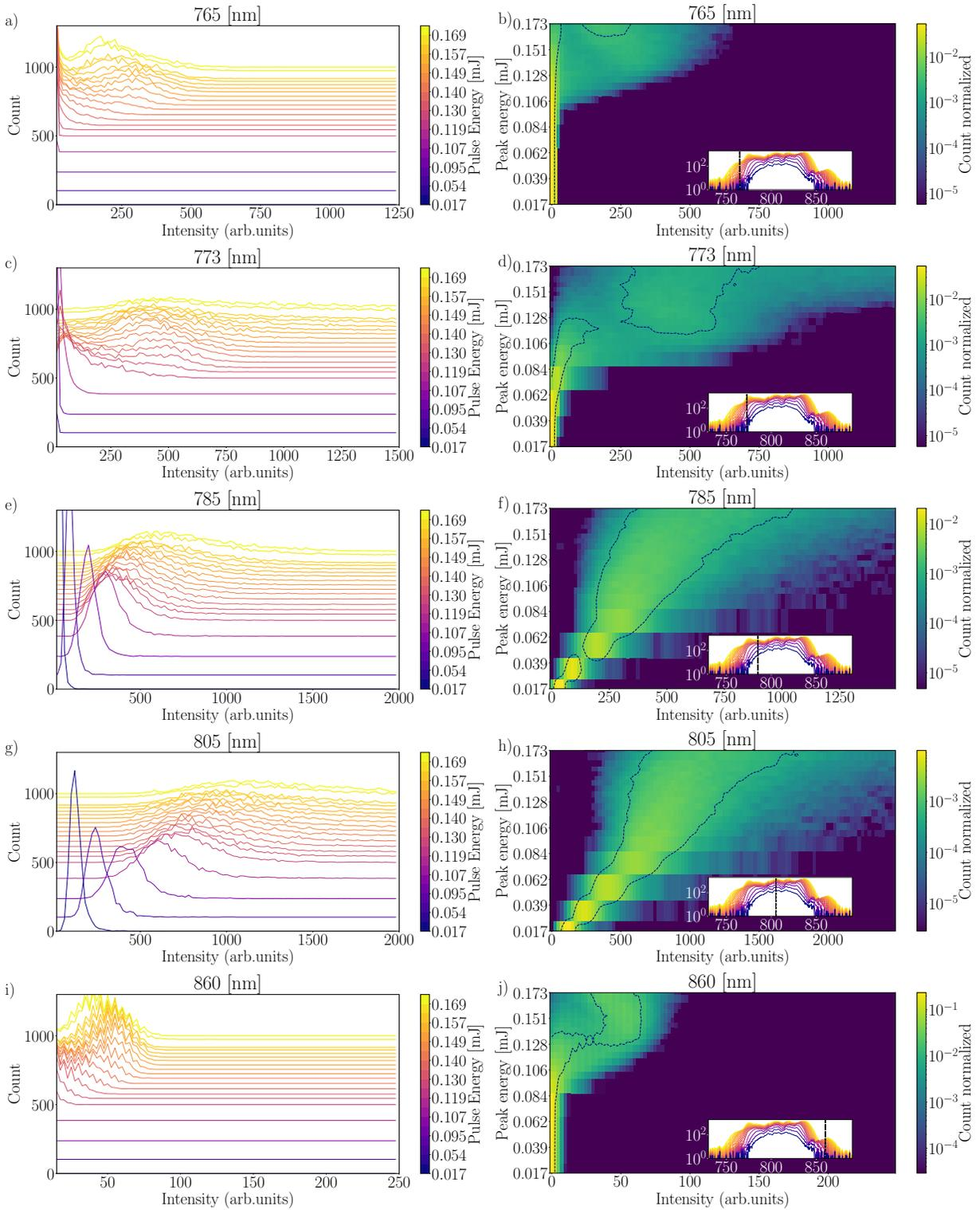


Figure 3. Evolution of the histogram of the spectral intensity at (a,b) 765 nm (transition through a bimodal distribution), (c,d) 773 nm (intermediate regime), (e,f) 785 nm, (g,h) 805 nm (smooth offset of the peak), and (i,j) 860 nm (bimodal transition). (a,c,e,g,i): Individual histograms for increasing incident pulse energies. The color scale is the same as in fig. 2. (b,d,f,h,j): Colormap of the same data. Each histogram is normalised to 1. Insets display the position of the wavelength in the spectrum (See also Figure 2a)

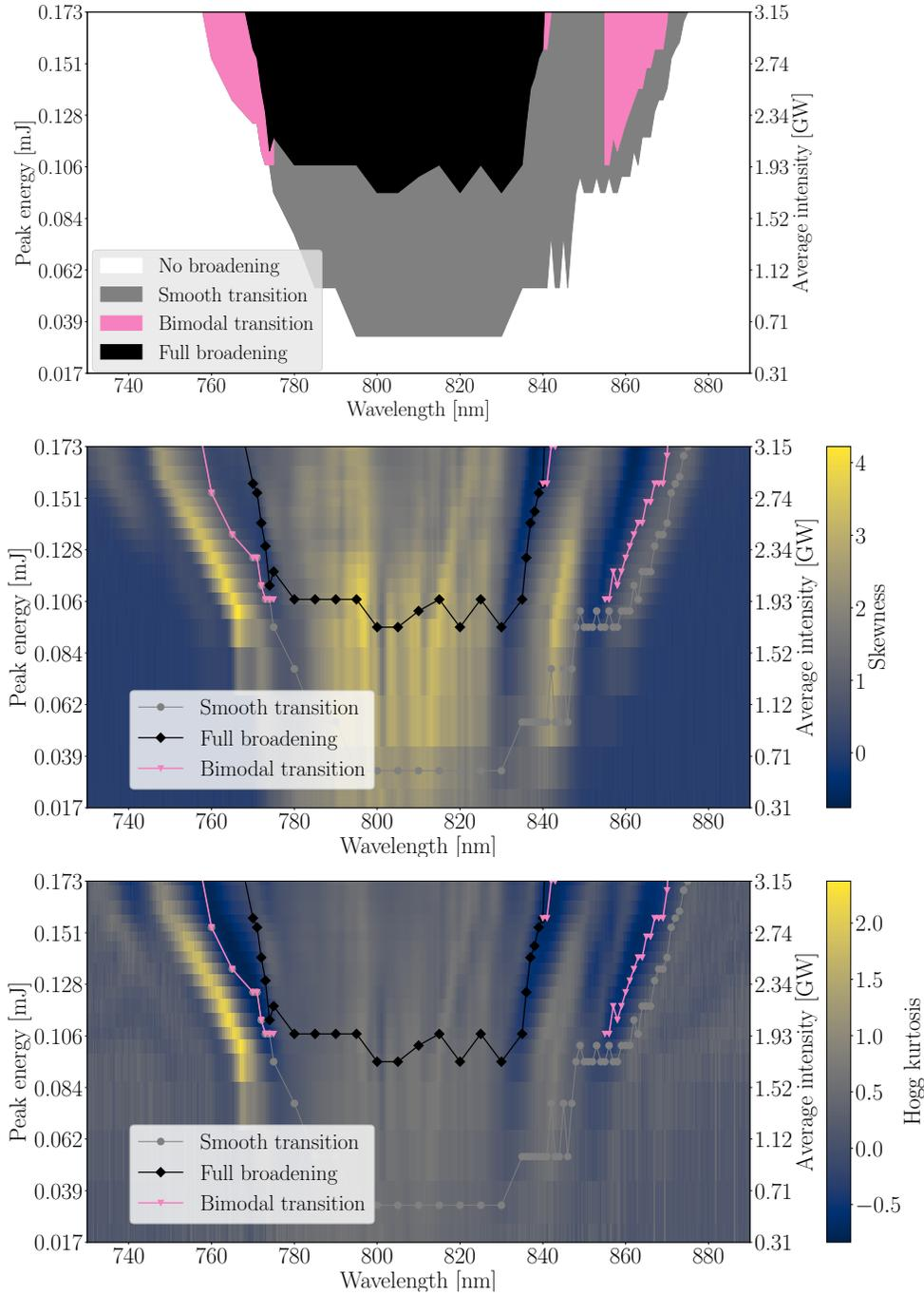


Figure 4. (a) "Phase diagram" displaying the different regimes as a function of wavelength and incident pulse energy, from non-broadened to fully-broadened, with continuous and bimodal transition modes in between. (b, c) Borders of the same diagram overlaid on (b) the skewness and (c) the Hogg's unbiased kurtosis estimator [37].

IV. CONCLUSION

In summary, we characterized the evolution of intensity fluctuations across the spectrum of an ultrashort beam propagating in air, for a wide range of powers covering below and up to the critical power for filamentation. While on the edges of the spectrum the transition to filamentation is discontinuous and displays a bimodal distribution of spectral intensities around the critical power, it is continuous around the fundamental incident laser wavelength. This dual behavior provides an explanation for the lack of unambiguous definition of the edges of the filamentation regime

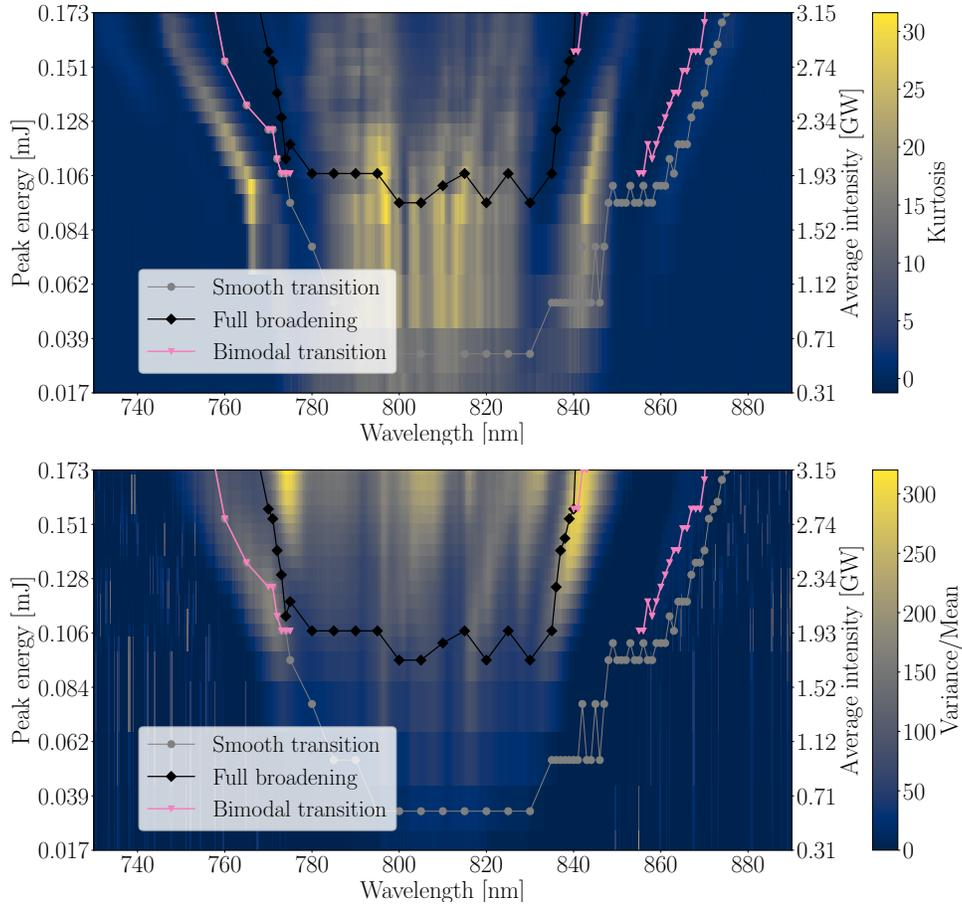


Figure 5. "Phase diagram" displaying the different regimes as a function of wavelength and incident pulse energy, from non-broadened to fully-broadened, with continuous and bimodal transition modes in between overlaid on (a) the kurtosis and (b) the the coefficient of variation (variance/mean).

in experiments or numerical simulations in spite of the intuitive understanding that filamentation qualitatively differs from a more linear propagation regime.

Funding. Swiss National Science Foundation (SNF, grant 200020-175697)

Acknowledgements. Experimental support was provided by Michel Moret.

Disclosures. The authors declare no conflicts of interest.

-
- [1] A. Braun, C. Y. Chien, S. Coe, and G. Mourou, *Optics communications* **105**, 63 (1994).
 - [2] S. Chin, F. Théberge, and W. Liu, *Applied Physics B* **86**, 477 (2007).
 - [3] A. Couairon and A. Mysyrowicz, *Physics Reports* **441**, 47 (2007).
 - [4] L. Bergé, S. Skupin, R. Nuter, J. Kasparian, and J.-P. Wolf, *Reports on progress in physics* **70**, 1633 (2007), arXiv: physics/0612063.
 - [5] P. Béjot, J. Kasparian, S. Henin, V. Loriot, T. Vieillard, E. Hertz, O. Faucher, B. Lavorel, and J.-P. Wolf, *Physical Review Letters* **104**, 103903 (2010).
 - [6] M. Rodriguez, R. Bourayou, G. Méjean, J. Kasparian, J. Yu, E. Salmon, A. Scholz, B. Stecklum, J. Eislöffel, U. Laux, A. P. Hatzes, R. Sauerbrey, L. Wöste, and J.-P. Wolf, *Physical Review E* **69**, 036607 (2004).
 - [7] M. Durand, A. Houard, B. Prade, A. Mysyrowicz, A. Durécu, B. Moreau, D. Fleury, O. Vasseur, H. Borchert, K. Diener, R. Schmitt, F. Théberge, M. Chateauneuf, J.-F. Daigle, and J. Dubois, *Optics Express* **21**, 26836 (2013).
 - [8] J. Kasparian, M. Rodriguez, G. Méjean, J. Yu, E. Salmon, H. Wille, R. Bourayou, S. Frey, Y.-B. André, A. Mysyrowicz, R. Sauerbrey, J.-P. Wolf, and L. Wöste, *Science* **301**, 61 (2003).
 - [9] X. M. Zhao, J.-C. Diels, C. Y. Wang, and J. M. Elizondo, *IEEE Journal of Quantum Electronics* **31**, 599 (1995).
 - [10] D. Comtois, C. Y. Chien, A. Desparois, F. Gérin, G. Jarry, T. W. Johnston, J. C. Kieffer, B. L. Fontaine, F. Martin,

- R. Mawassi, H. Pépin, F. A. M. Rizek, F. Vidal, P. Couture, H. P. Mercure, C. Potvin, A. Bondiou-Clergerie, and I. Gallimberti, *Applied physics Letters* **76**, 819 (2000).
- [11] J. Kasparian, R. Ackermann, Y.-B. André, G. Méchain, G. Méjean, B. Prade, P. Rohwetter, E. Salmon, K. Stelmaszczyk, J. Yu, A. Mysyrowicz, R. Sauerbrey, L. Wöste, and J.-P. Wolf, *Optics Express* **16**, 5757 (2008).
- [12] E. Schubert, D. Mongin, J. Kasparian, and J.-P. Wolf, *Optics Express* **23**, 28640 (2015).
- [13] E. Schubert, D. Mongin, J. Kasparian, and J.-P. Wolf, *Optics Express* **25**, 11210 (2017).
- [14] F. Théberge, J.-F. Daigle, J.-C. Kieffer, F. Vidal, and M. Châteauneuf, *Scientific Reports* **7** (2017), 10.1038/srep40063.
- [15] P. Sprangle, J. R. Peñano, B. Hafizi, and C. A. Kapetanacos, *Physical Review E* **69** (2004).
- [16] A. Houard, Y. Liu, B. Prade, V. T. Tikhonchuk, and A. Mysyrowicz, *Physical Review Letters* **100**, 255006 (2008).
- [17] A. G. Stepanov, S. Henin, Y. Petit, L. Bonacina, J. Kasparian, and J.-P. Wolf, *Applied Physics B* **101**, 11 (2010), doi:10.1007/s00340-010-4186-4.
- [18] A. G. Stepanov, S. Henin, Y. Petit, L. Bonacina, J. Kasparian, and J.-P. Wolf, *Applied Physics B-Lasers and Optics* **115**, 293 (2014), WOS:000334493900018.
- [19] J. Daigle, F. Théberge, M. Henriksson, T. Wang, S. Yuan, M. Châteauneuf, J. Dubois, M. Piché, and S. L. Chin, *Optics Express* **20**, 6825 (2012).
- [20] M. Clerici, M. Peccianti, B. E. Schmidt, L. Caspani, M. Shalaby, M. Giguère, A. Lotti, A. Couairon, F. Légaré, T. Ozaki, D. Faccio, and R. Morandotti, *Physical Review Letters* **110**, 253901 (2013).
- [21] L. de la Cruz, E. Schubert, D. Mongin, S. Klingebiel, M. Schultze, T. Metzger, K. Michel, J. Kasparian, and J.-P. Wolf, *Applied Physics Letters* **109**, 251105 (2016).
- [22] G. Schimmel, T. Produit, D. Mongin, J. Kasparian, and J.-P. Wolf, *Optica* **5**, 1338 (2018).
- [23] S. Henin, Y. Petit, P. Rohwetter, K. Stelmaszczyk, Z. Hao, W. Nakaema, A. Vogel, T. Pohl, F. Schneider, J. Kasparian, K. Weber, L. Wöste, and J. Wolf, *Nature Communications* **2**, 456 (2011).
- [24] J. Ju, J. Liu, C. Wang, H. Sun, W. Wang, X. Ge, C. Li, S. L. Chin, R. Li, and Z. Xu, *Optics Letters* **37**, 1214 (2012).
- [25] J. Yu, D. Mondelain, J. Kasparian, E. Salmon, S. Geffroy, C. Favre, V. Boutou, and J. P. Wolf, *Applied Optics* **42**, 7117 (2003).
- [26] O. Lahav, L. Levi, I. Orr, R. A. Nemirowsky, J. Nemirowsky, I. Kaminer, M. Segev, and O. Cohen, *Physical Review A* **90**, 021801 (2014).
- [27] N. Jhajj, E. W. Rosenthal, R. Birnbaum, J. K. Wahlstrand, and H. M. Milchberg, *Physical Review X* **4**, 011027 (2014).
- [28] S. L. Chin, Y. Chen, O. Kosareva, V. P. Kandidov, and F. Théberge, *Laser Physics* **18**, 962 (2008).
- [29] K. Lim, M. Durand, M. Baudelet, and M. Richardson, *Scientific Reports* **4** (2015), 10.1038/srep07217.
- [30] D. Reyes, M. Baudelet, M. Richardson, and S. Rostami Fairchild, *Journal of Applied Physics* **124**, 053103 (2018).
- [31] D. R. Solli, C. Ropers, P. Koonath, and B. Jalali, *Nature* **450**, 1054 (2007), 10.1038/nature06402 0028-0836.
- [32] J. Kasparian, P. BÉjot, J.-P. Wolf, and J. M. Dudley, *Optics Express* **17**, 12070 (2009).
- [33] R. W. Boyd, *Nonlinear Optics*, 3rd ed. (Academic Press, Boston, 2008).
- [34] R. Ackermann, G. Méjean, J. Kasparian, J. Yu, E. Salmon, and J.-P. Wolf, *Optics Letters* **31**, 86 (2006).
- [35] R. Salamé, N. Lascoux, E. Salmon, J. Kasparian, and J. P. Wolf, in *2nd French-Chinese Workshop on "Ultra-short and Ultra-intense Lasers and Applications (FCILA-2007)* (2007).
- [36] E. Schubert, L. de la Cruz, D. Mongin, S. Klingebiel, M. Schultze, T. Metzger, K. Michel, J. Kasparian, and J.-P. Wolf, *Physical Review A* **94**, 043808 (2016).
- [37] T. H. Kim and H. White, *Finance Research Letters* **1**, 56 (2004).